46th AIAA/ASME/SAE/ASEE Joint Propulsion Conference & Exhibit
25 - 28 July 2010, Nashville, TN

AIAA 2010-7107

A Plasma Propulsion Concept Based on Direct Ion Acceleration with Beating Electrostatic Waves

B. Jorns * and E.Y. Choueiri†

Electric Propulsion and Plasma Dynamics Laboratory, Princeton University, Princeton, NJ, 08544

A new concept for plasma propulsion that relies on using beating electrostatic wave (BEW) direct ion acceleration to augment the linear ion current produced in a plasma by a rectilinear, magnetic slope configuration is presented and analyzed. The types of particle trajectories possible in a magnetic slope configuration are identified and shown to produce a net flow in a thermalized ion ensemble. The ability of BEW to augment this flow in the magnetic null direction by direct acceleration, as opposed to ion heating, is subsequently demonstrated and a thruster concept that relies on this process is described. It is expected that the direct ion acceleration would yield a propulsive performance that is superior to that obtained by concepts that rely on plasma heating, which suffer from relatively high wall losses.

Nomenclature

r_L	Larmor radius
$v_\perp$	Perpendicular velocity of ions
ρ	Normalized Larmor radius
ω_c	Ion cyclotron frequency
ω_i	Wave frequency of i^{th} wave
τ	Time normalized by ion cyclotron frequency
ν	Normalized wave frequency
L	Length scale of acceleration region
δ	Half-width of magnetic slope
x, y_{GC}	Coordinates of guiding center
$\mathbf{B}$	Magnetic field
θ	Larmor angle
$p_{x,y}$	Canonical momenta
A_x	Magnetic potential
h	Full Hamiltonian
H	Unperturbed Hamiltonian
k	Wavenumber
E	Electric field amplitude
ν_c	Ion collision frequency

I. Introduction

In the late 1970s, a series of atmospheric sounding rockets revealed a naturally occurring ion acceleration mechanism at an altitude of 1000 km in the topside ionosphere.[1,2] Magnetized ions were observed to experience prodigious increases in energy through nonlinear interactions with waves in regions of electrostatic turbulence. Uncharacteristically for wave-particle interactions, however, ions with initial velocity well below

*Graduate Student, Research Assistant
†Chief Scientist, EPPDyL, Professor, Applied Physics Group, AIAA Fellow

the phase velocity of the exciting waves were observed to be accelerated. In 1998, Ram *et al* proposed an interaction with a spectrum of multiple electrostatic waves propagating perpendicularly to the magnetic field could be responsible for this non-resonant acceleration.[3] In this same same year, Benisti *et al* showed the necessary condition for this acceleration to occur is that at least two of the waves differ in frequency by an integer multiple of the cyclotron frequency:[4,5]

$$\omega_2 - \omega_1 = n\omega_c \tag{1}$$

where ω_1 and ω_2 are the angular frequencies of the exciting waves, ω_c is the ion cyclotron frequency, and n is an integer. Spektor and Choueiri in a subsequent analytical investigation showed that this criteria for acceleration is necessary but not sufficient.[6] Rather, the beating condition must be satisfied while the ion's initial Hamiltonian must fall within a certain range in order to insure acceleration. While this limited the scope of BEW acceleration, the mechanism still retained the property of accelerating low energy ions. This is in stark contrast to single electrostatic wave (SEW) heating described in detail by Karney as well as other resonant processes, and it is for this reason that there has been significant interest in the BEW mechanism.[7] In particular, most applications of the BEW mechanism to date have focussed on plasma heating with BEW electrostatic waves as its ability to accelerate low energy ions makes it an efficient alternative to resonant processes.[8–11] In this respect, BEW plasma heating has a possible application in electric propulsion as a heating stage for an electrothermal or magnetic nozzle concept.

While on-going work investigates this possibility in both optimizing and fully characterizing the BEW process, the unique effect the BEW mechanism has on individual particle dynamics can be adapted to produce direct linear acceleration. The concept, of course, of producing linear particle acceleration through a plasma wave interaction is not new. RF current drive, for example, can generate prodigious current through an RF interaction (see Ref. 12 for a comprehensive review of the subject) . However, while these mechanism rely on a resonant interaction of particles with the wave velocity and subsequent diffusion of energy in velocity phase space through collisional processes, the ability of BEW acceleration to coherently accelerate ions with arbitrarily low initial energy opens new possibilities for directed acceleration. It is the goal of this investigation to characterize in detail a thruster concept that relies on a magnetic slope to exploit the unique features of the BEW mechanism.

To this end, we have organized this paper in the following way. In the first section, we provide a review of the equations of motion for a single ion subject to beating electrostatic waves with a geometry chosen to be easily applied to a thruster design. In the next section, we restrict our analysis to the unperturbed case (no waves) and classify the different types of ion trajectories possible in a magnetic slope. We then use these results to show a thermalized ion ensemble will experience a net drift in the presence of a magnetic slope. Following this, we demonstrate that BEW acceleration can augment this drift in a way advantageous to traditional heating methods. In the final section, we outline a proof of concept design experiment to investigate the application of the enhanced BEW ion flow to a thruster concept.

II. Single Ion Dynamics

For this investigation, we define a simplified geometry for ion motion shown in Figure 1 where we take the magnetic field to be $\mathbf{B} = B(y)\hat{z}$ direction and the electrostatic waves to propagate in the $\hat{x}$ direction with wavenumber k. We further define a steep slope in the magnetic field that occurs in the y-direction from $y = \pm\delta$ and changes polarity at $y = 0$. Outside the magnetic slope, the field is assumed to be constant such that $|B(|y| > \delta)| = B_0$. These criteria are combined in a general expression as

$$B(y) = B_0 f(y) \tag{2}$$

where

$$f(y) = \begin{cases} -1 & \text{if } y \leq -\delta; \\ 1 & \text{if } y \geq \delta; \\ 0 & \text{if } y = 0; \end{cases}$$

and

$$f'(y) > \quad 0 \quad \text{if } -\delta \leq y \leq \delta$$

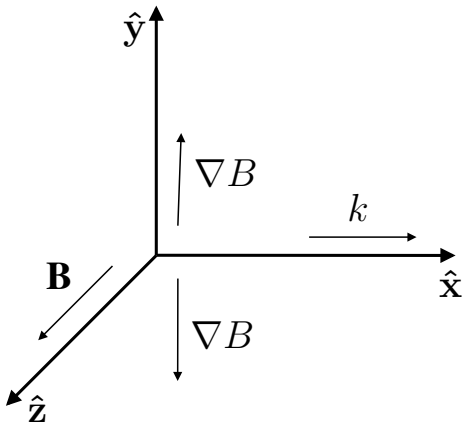

Figure 1. The geometry of this investigation where the wavevector k is defined to be in the $\hat{x}$, the magnetic field, B, is in the $\hat{z}$ direction, and the gradient of the magnetic field in both cases points away from the region of null magnetic field at $y = 0$.

and continuity is enforced. We show an example of a magnetic field that satisfies the above criteria in Figure 2. This particular configuration is described by the equation

$$B = B_0 \tanh \frac{3y}{\delta} \tag{3}$$

where the factor of 3 ensures that at $y = \pm\delta$, the magnetic field will be nearly unity. For all subsequent numerical results, we employ this field.

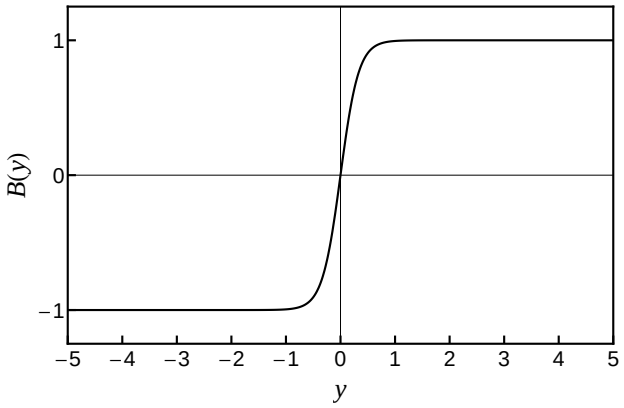

Figure 2. Magnetic slope as described by Eq. 3 for $\delta = 1$. The magnetic null occurs at $y = 0$ while the region is homogenous for $|y| > 1$

With this description of the field, we are now free to re-derive the equations of motion for an ion subject to beating electrostatic waves. For this purpose, we adapt the initial derivations for the interaction of an ion with multiple electrostatic waves performed by Chia.[13] In the presence of a magnetic field and electric potential, the Hamiltonian governing the equations of motion for a single ion is given by

$$h = (\mathbf{p} - q\mathbf{A})^2 + q\phi \tag{4}$$

where $\mathbf{p}$ is the canonical momenta, $\mathbf{A}$ is the magnetic vector potential, q is the charge, and ϕ is the electrostatic potential. Since $\nabla \times \mathbf{A} = \mathbf{B}$ and $\mathbf{B} = B(y)\hat{z}$, we can without loss of generality let $A_y = A_z = 0$ and $A_x(y) = -\int_0^y B(y')dy'$. We further define the electric field generated by the beating electrostatic waves to be

$$\mathbf{E} = \sum_{i=1,2} E_0 \sin(kx - \omega_i t)\hat{x} \tag{5}$$

where E is the electric field amplitude, k is the wavenumber, and ω_i is the frequency of the i^{th} wave defined in such a way to satisfy the beating criterion of Eq. 1 for $n = 1$ ($\omega_2 - \omega_1 = \omega_c$). We have in this case assumed the waves have the same initial phase, wave number, and amplitude. This has been shown to yield the largest single ion acceleration.[5] We further assume that k and E_0 are constant for this investigation.

For our time independent magnetic field, we have $\nabla\phi = -\mathbf{E}$ such that

$$\phi = \sum_{i=1,2} \frac{E_0}{k} \cos(kx - \omega_i t). \tag{6}$$

Therefore, the Hamiltonian governing the single ion dynamics is given by

$$h = \frac{1}{2}\left(\left[p_x - qA_x\right]^2 + p_y^2\right) + \frac{qE_0}{k} \sum_{i=1,2} \cos(kx - \omega_i t) \tag{7}$$

where $p_x = m\dot{x} + qA_x$, $p_y = m\dot{y}$ and m is the particle mass. We in turn normalize this expression following the convention of Spektor and Choueiri to yield the canonical transformation:[6]

$$h = \frac{1}{2}\left(\left[P_X - \overline{A}_X\right]^2 + P_Y^2\right) + \varepsilon \sum_{i=1,2} \cos(X - \nu_i \tau) \tag{8}$$

where

$$\tau = \omega_c t \qquad h = \tfrac{\omega_c^2 m}{k} H; \qquad \nu_i = \omega_i/\omega_c; \qquad \varepsilon_i = \tfrac{qkE_i}{m\omega_c^2}; \quad kx = X; \qquad ky = Y$$

$$P_X = \dot{X} + \overline{A}_X; \quad \overline{A}_X = \tfrac{qk}{m\omega_c} A_x(Y/k); \quad P_Y = \dot{Y}; \quad \nu_1 = \nu; \quad \nu_2 = \nu + 1$$

where $\omega_c = qB_0/m$ is the magnitude of the ion cyclotron frequency in the regions of constant magnetic field, $|y| > \delta$. Physically, Eq. 8 describes the evolution of the normalized position and velocity of the ion subject to BEW. In the following section, we analyze this Hamiltonian first in the case where $\varepsilon = 0$ and categorize different types of ion motion. We then explore where $\varepsilon \neq 0$ and how it influences ion orbit in our magnetic field configuration.

III. Unperturbed Orbits ($\varepsilon = 0$)

In this section, we use Eq. 8 in conjunction with energy considerations in order to categorize ion behavior. This is similar to the approach employed by Landsman *et al* in their investigation of single ion orbits in a field reserved configuration.[14] We write Eq. 8 in the $\varepsilon = 0$ case such that

$$H = \frac{1}{2}\left(\left[P_X - \overline{A}_X\right]^2 + P_Y^2\right). \tag{9}$$

This expression reveals that both P_X and H are constants of motion. In particular, H is the total energy of the system characterized by an effective potential:

$$V_{eff} = \frac{1}{2}\left(\left[P_X - \overline{A}_X\right]^2\right). \tag{10}$$

By using $\delta = 1$ and $k = 1$ to evaluate $\overline{A}_X$ in the above expression, we illustrate in Figure 3 the two possible forms this potential can take. For $P_X < 0$, V_{eff} is a single well symmetric about $Y = 0$. For $P_X > 0$, the potential becomes a double well with minima that intersect the axis. We consider each case separately and the resulting ion motion.

I. For this case of $P_X > 0$, we show two orbits in Fig. 4 at $H = 17.2$ and 94.8, which are characteristic of all trajectories for $P_X > 0$. Specifically, these orbits have a guiding center of motion that is in the region of opposite polarity and approximately beyond the magnetic slope such that the orbit completes less than half of its Larmor rotation before intersecting the magnetic slope region. As the ion's momentum carries it across the magnetic null, it experiences a reversal in the direction of gyration. The net effect of this is a linear translation in the $\hat{x}$ direction, which as can be seen from Ref. 14, is the linear analog

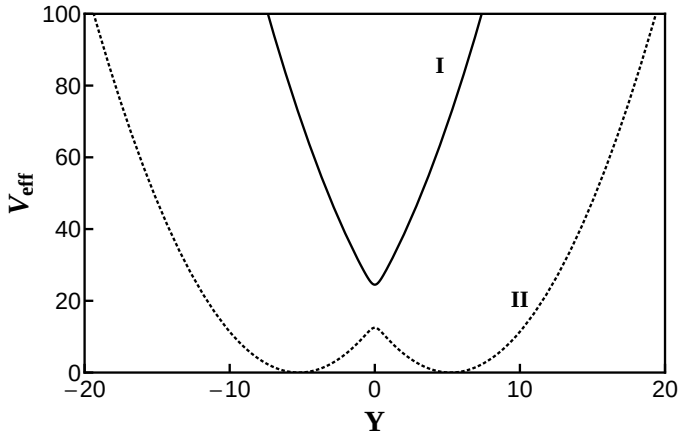

Figure 3. Two cases for the effective potential V_{eff} evaluated with Eq. 10 for $k = \delta = 1$. Case I, the solid line, has $P_X = 8$ and is characterized by single well. Case II, the dotted line, corresponds to $P_X = -5.8$ and has two potential wells.

to the "betatron orbits" defined for the Field Reserved Configuration (FRC). It is for this reason we refer to these trajectories as "linear betatron" (LB) orbits. As a final observation, we note from Figs. 4(a) and 4(b) that with increasing H, the effective guiding center moves further away from the magnetic null such that the ion completes a decreasingly smaller fraction of its Larmor precession before reaching the magnetic null. This results in a faster and more linear motion in the $\hat{x}$ direction.

II. We show in Fig. 5 six characteristic orbits that serve to illustrate the possible trajectories in the regime where $P_X < 0$. For small initial energy, Figure 5(a) , the ion energy places it near the one of the minima of the effective potential, V_{eff}, and at sufficiently low values, this potential is symmetric about each minimum. As a consequence, ion motion is characterized by simple Larmor precession. For slightly larger values of initial energy, Fig. 5(b), the potential exhibits asymmetry about the potential minima, though the ion energy is sufficiently small that it does not escape the well. Therefore, the Y value of the orbit maintains its sign, and the ion undergoes a grad-B drift in the $-\hat{x}$ direction. Physically, this trajectory is the consequence of the ion orbit barely moving the particle into the magnetic slope region. For Figs. 5(c) and 5(d), the ion has sufficient energy to cross the magnetic null. This is reflected in energy space as the ion having sufficient energy to overcome the potential barrier at $Y = 0$ from Figure 3 and therefore move into the region of opposite polarity. As it crosses the magnetic field region, the particle reverses the direction of gyration and traces out what is termed a "figure-8" orbit.[14] At the lower energy case, Fig. 5(c), we see the "figure-8" drifts in the $-\hat{x}$ direction, whereas at the higher value case, Fig. 5(d), the drift is in the $\hat{x}$ direction. Finally, in Figs. 5(e) and 5(f), for progressively higher values of energy, the "figure-8" orbits open up and approach the LB trajectories of Case I.

We can derive the exact conditions under which each type of orbit occurs with an analysis of Eq. 10. First, we see an ion will only become trapped in simple Larmor precession or a grad-B drift on one side of the magnetic slope if the total energy H places it below the peak that occurs in the potential at $Y = 0$. This condition is expressed as

$$H < V_{eff}(0). \tag{11}$$

As we outlined in Case II, the transition from cyclotron motion to grad-B drifts occurs when the potential well begins to exhibit asymmetry about the minima. For the ideal, piecewise defined magnetic field defined in Sec. II, we see this asymmetry begins right at the boundary of the magnetic slope $|Y| = k\delta$. Therefore, we can resolve further the energy space of trapped orbits by defining the criterion for simple Larmor precession:

$$0 < H < V_{eff}(k\delta) \tag{12}$$

and grad-B drifts:

$$V_{eff}(k\delta) < H < V_{eff}(0). \tag{13}$$

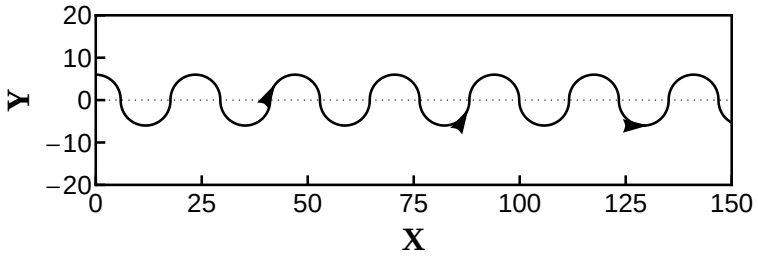

(a) H = 17.2 and $P_X = 0.1$

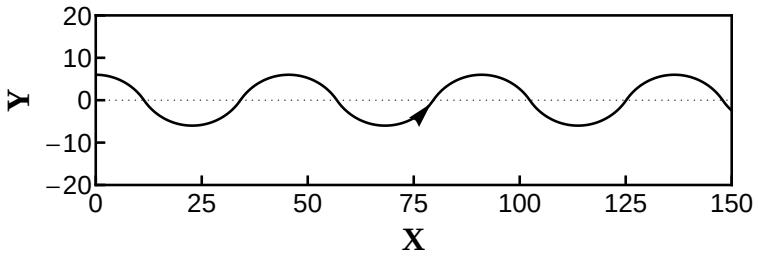

(b) H = 94.8 and $P_X = 8$

Figure 4. Characteristic ion trajectories for $P_x > 0$ and increasing values of H. The net motion is in the $\hat{x}$ and the trajectories become more elongated and therefore parallel to the $\hat{x}$ axis for higher energies, H.

We see for arbitrary $f(y)$ that satisfy the criteria outlined in Sec. II, $A_X \leq 0$ such that the above expressions imply grad-B and cyclotron drift only occur when $P_X < 0$. Now, it is evident that the opposite of this criteria should lead to ion trajectories that cross the magnetic null region at $Y = 0$ and thus become figure-8 or LB orbits. As we saw in Figs. 5(c) and 5(d), however, it is possible that the figure-8 orbit will lead to precession in either the positive or negative $\hat{x}$ direction. We derive in the Appendix the approximate condition for the "backward figure-8" trajectories (in the $\hat{x}$ direction):

$$V_{eff}(0) < H < \frac{1}{2}\left(P_X - \overline{A}_X(k\delta) - k\delta/2\right)^2. \tag{14}$$

This thus implies the "forward figure-8" (in the $\hat{x}$ direction) orbits occur where

$$\frac{1}{2}\left(P_X - \overline{A}_X(k\delta) - k\delta/2\right)^2 > H; \qquad P_X \leq 0, \tag{15}$$

and our LB orbits are at

$$P_X > 0. \tag{16}$$

With these expressions, we have characterized the full spectrum of single ion motion for a magnetic field described by a function $f(y)$ and in the unperturbed case ($\varepsilon = 0$). These compiled results are depicted graphically in Figure 6(a) where we have classified each type of ion trajectory as it depends on the constants of motion.

We can also recast H and P_X and the criteria shown in Fig. 6(a) in terms of more physically intuitive variables—namely the Larmor radius and guiding center of motion. To this end, we consider the term

$$X_{GC} = X + \frac{B}{|B|}\dot{Y} = X + \frac{B}{|B|}P_Y \tag{17}$$

Taking the time derivative, we find

$$\dot{X}_{GC} \quad = \quad \dot{X} - \frac{B}{|B|}\left(P_X - \overline{A}_X(Y)\right)\overline{A}'_X(Y)$$

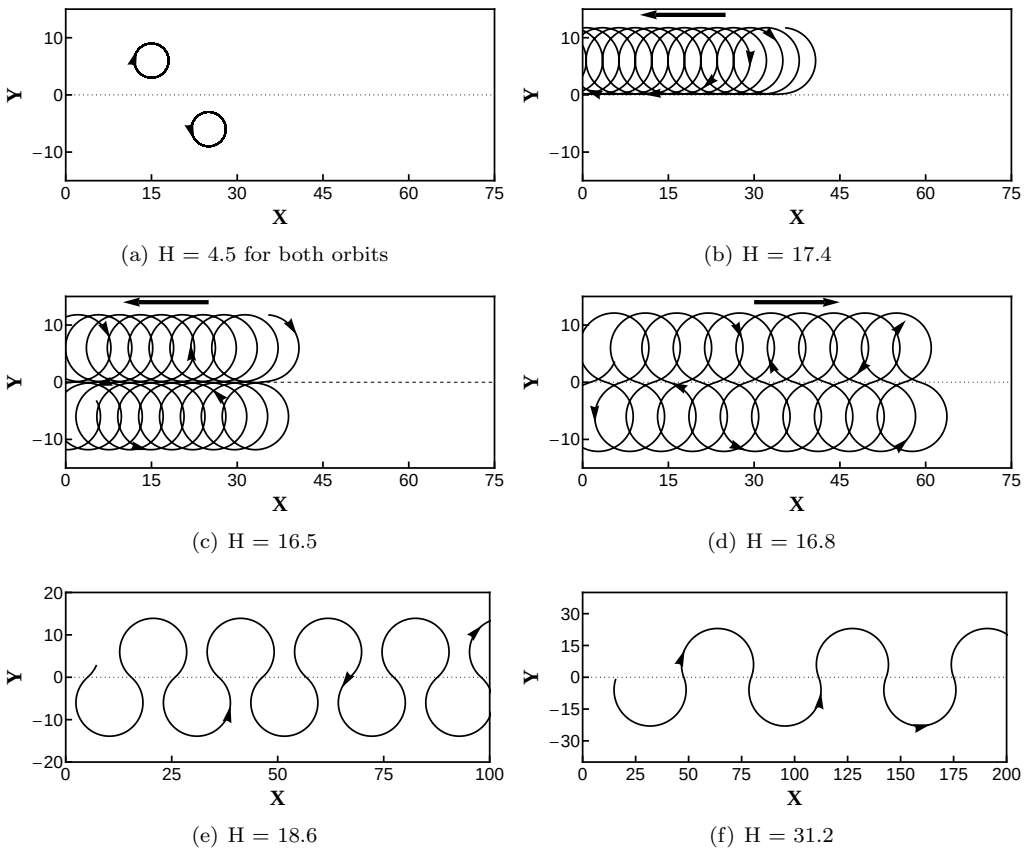

(a) H = 4.5 for both orbits

(b) H = 17.4

(c) H = 16.5

(d) H = 16.8

(e) H = 18.6

(f) H = 31.2

Figure 5. Characteristic ion trajectories for $P_x = -5.8$ and increasing values of H. The time interval is the same for each orbit. Where necessary for clarification, the bold arrows indicate the net motion of the guiding center.

$$= \dot{X}\left(1 - \frac{B}{|B|}\overline{A}'_X(Y)\right) \tag{18}$$
$$= \dot{X}\left(1 - \frac{B}{|B|}f(Y/k)\right)$$

where we have used the definition of P_X and $\overline{A}_X$. If we make the assumption that $|Y| > k\delta$, we see the equation yields $\dot{X}_{GC} = 0$. In other words, X_{GC} is a constant of a motion in the region outside of the magnetic slope. We take this assumption along with our definition of P_X to find

$$X = -\frac{B}{|B|}\dot{Y} + X_{GC} \tag{19}$$

$$Y = \frac{B}{|B|}\dot{X} + Y_{GC} \tag{20}$$

$$\tag{21}$$

where Y_{GC} is a constant related to P_X by

$$Y_{GC} = -\frac{B}{|B|}\left(P_X - \overline{A}_X(k\delta) - k\delta\right). \tag{22}$$

Eq. 19 thus shows the expected result that in the uniform magnetic field region $|Y| > k\delta$, the ion motion is described by Larmor precession such that

$$X = \rho\sin\theta + X_{GC} \tag{23}$$

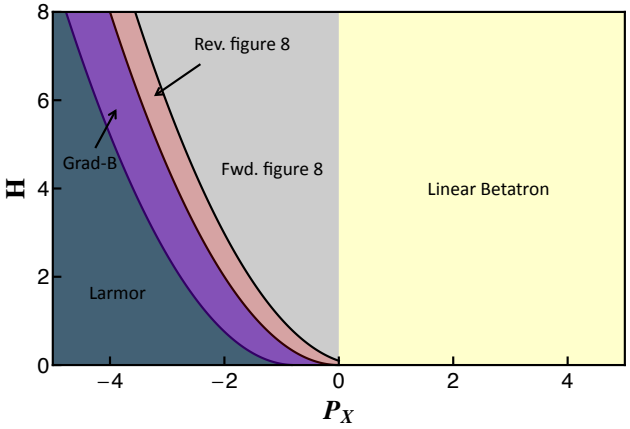

(a) H = 17.2 and $P_X = 0.1$

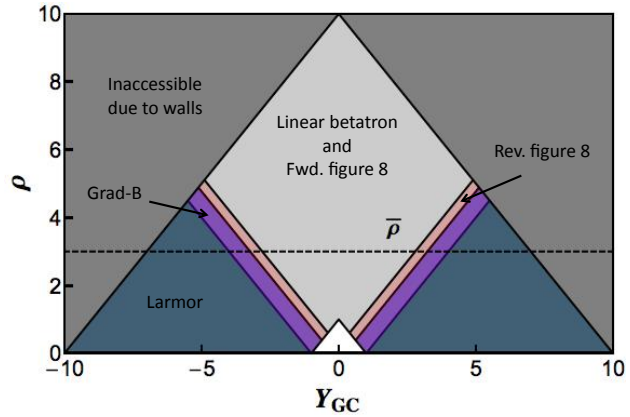

(b) Orbit classification in physical space. The white triangle denotes the values where the expression for Y_{GC} from Eq. 22 is not valid.

Figure 6. Classification of orbits for our linear configuration with a magnetic slope. $k = \delta = 1$

$$Y = \frac{B}{|B|}\rho\cos\theta + Y_{GC} \tag{24}$$

where $\rho = kr_L = \sqrt{\dot{X}^2 + \dot{Y}^2}$ is the normalized Larmor radius, (X_{GC}, Y_{GC}) is the location of the normalized guiding center, and θ is the Larmor angle measured from the $\mathbf{B} \times \mathbf{k}$ direction. Finally, with our definitions for P_X and P_Y, we find

$$\begin{aligned} H &= \frac{1}{2}\left(\dot{X}^2 + \dot{Y}^2\right) \\ &= \rho^2/2. \end{aligned} \tag{25}$$

For any ion with initial position outside of the magnetic slope, Eqs. 22 and 25 provide us with a way to relate the physical parameters of the orbit–its Larmor radius and Y-coordinate of the guiding center– to the energy H and canonical momentum P_X. We thus can express the map from Fig. 6(b) in terms of ρ and Y_{GC} in Fig. 6(b). For simplicity, we have combined all $\hat{x}$ drifting orbits (LB and forward figure-8) into one region (gray) in this trajectory map. We further note that this description is only valid, as described in the derivation above, if $|Y_0| > k\delta$ where Y_0 denotes the initial value of the the Y coordinate of the ion. It is for this reason that the white triangle appears in the figure.

IV. Linear acceleration of an ion ensemble

With the classification of ion behavior in terms of physical coordinates provided in the previous section, we now pose the central question: can this magnetic slope produce a preferential linear acceleration in an ensemble? In order to address this, we consider the velocity and space probability distribution of an ion ensemble in the plane perpendicular direction to **B** which we denote

$$F(v_x, v_y, x, y). \tag{26}$$

We make three assumptions about this distribution. First, the ensemble is isotropic in physical space. Second, ions are magnetized such that $\omega_c \gg \nu_c$ where ν_c is the collision frequency of the ions. And third, we assume that $L \gg \delta$ where L denotes the length scale of the set up in the $\hat{y}$ direction. This last assertion coupled with the first assumption show us that

$$\frac{\int_{-\delta}^{\delta} F(v_x, v_y, x, y)dy}{\int_{-L}^{L} F(v_x, v_y, x, y)dy} \ll 1. \tag{27}$$

In other words, the fraction of ions at any given time in the magnetic slope region is very small. Therefore, the majority of particles are magnetized with the same magnitude field B_0, which reduces the probability distribution to approximately $f(v_\perp)$ where $v_\perp = \sqrt{\dot{x} + \dot{y}^2}^2$ and we have integrated over the isotropically distributed spatial coordinates. With this description of the plasma, we can calculate the average, normalized radius of the ions:

$$\overline{\rho} = \frac{v_\perp k}{\omega_c} = \frac{k}{\omega_c} \int v_\perp f(v_\perp) dv_\perp \tag{28}$$

We plot a representative value of $\overline{\rho}$ in Fig. 6(b) which appears as a straight line due to the isotropy in Y. This figure also includes the effects of a closed geometry. Specifically, we approximate walls in the $\hat{y}$ direction as the condition that ions must have $|Y_{GC}| + \rho < kL$ where L is the length of the experiment as defined above. With this added effect, we see from Fig. 6(b) that for those particles within the closed geometry, an ensemble at equilibrium will have a fraction of ions follow each type of trajectory. Moreover, for sufficiently large values of $\overline{\rho}$ there will be more ions subject to $\hat{x}$ drifts rather than $-\hat{x}$ drifts, and since the fraction of ions present in the Larmor region do not have a net motion, an ion flow subsequently will form along the magnetic null in the $\hat{x}$ direction. This linear analog to the azimuthal current found in the FRC configuration[14,15] thus shows us that without a magnetic nozzle, a magnetic slope can produce directed, linear acceleration from a plasma. And with this observation, we have described the means to generate directed thrust for a plasma thruster concept. It is also evident that for the purposes of achieving an effective and efficient concept, we can *augment* this flow by increasing the fraction of ions subject to forward-drifting orbits. We discuss three methods for achieving this end: ion heating, changing the magnetic field topography, and coherent ion acceleration.

1. Ion Heating

The most intuitive way to increase the fraction of ions in the forward-drifting region is to raise $\overline{\rho}$. Thermal ion heating can produce this result by increasing the average perpendicular velocity $\langle v_\perp \rangle$. This must be done with care, however, for as we increase $\overline{\rho}$, it is evident that the ions become less magnetized and are more prone to escape to the walls. Indeed, it is only in the neighborhood of the point where the inaccessible region just intersects the LB and figure-8 region in Fig.6(b) where we qualitatively expect the fastest ion population along the magnetic null. Increasing $\overline{\rho}$ further would start to reduce the fraction of ions in the accelerated region.

2. Magnetic field topography

The second method for increasing the number of ions subject to LB and figure-8 orbits is to change $\overline{\rho}$ by decreasing ω_c, i.e. lowering the background, uniform magnetic field. This, however, requires the same considerations as ion heating. On the the other hand, we could expand the magnetic slope region by increasing δ. This has the effect of "widening" the LB and forward figure-8 region without the cost of demagnetizing the plasma. Changing δ thus can help augment ion acceleration for a given $\overline{\rho}$. However, we recognize that this factor is a fixed parameter of the system. Once we optimize it, we can no longer change it.

3. Coherent Ion Acceleration

While the two methods outlined above show promise for augmenting the ion flow, the limitations we discussed lead us to examine a third process. Specifically, instead of using a heating technique that relies on thermal equilibration to a higher $\overline{\rho}$, we propose the use of coherent ion acceleration. Such a mechanism that works on a reasonably fast time scale $t < \nu_c^{-1}$ will accelerates ions from Larmor regions to the forward drifting areas such that we would have a means of effectively lowering the bounds in Fig. 6(b) while avoiding the deleterious effects of demagnetizing the ions. In the next section, we show how beating electrostatic waves, BEW, are well suited as such an acceleration scheme.

V. BEW ion acceleration

In order to simplify our analysis, we restrict our consideration of BEW acceleration to ion dynamics in the homogenous magnetic field zone, $|Y| > ky$, and focus on determining what conditions will push the ions into the forward drifting region. To this end, as Eq. 8 shows, the introduction of BEW to the ion dynamics renders the equations of motion intractable. In order to analyze the behavior, therefore, it is necessary to turn to Poincaré cross-sections as well as perturbation theory methods. A significant body of work exists in performing these analyses, which we summarize here.[?,5,6,13,16] Specifically, Spektor and Choueiri using

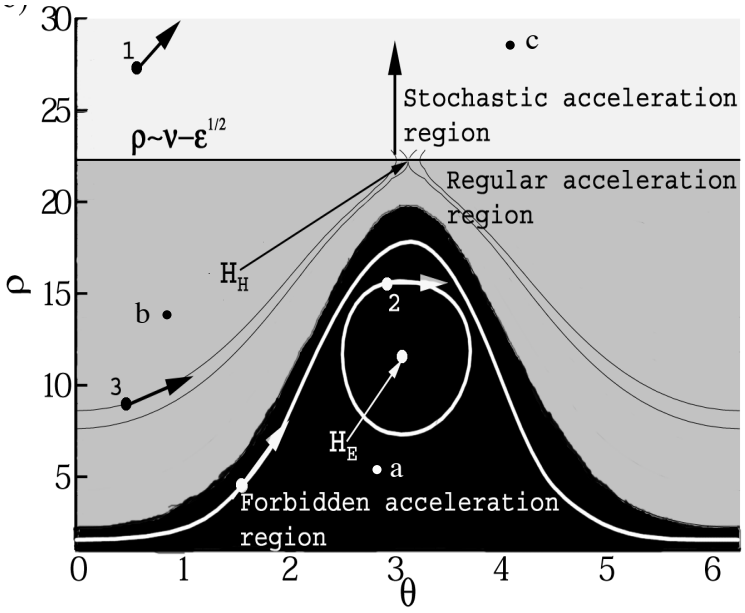

Figure 7. Poincaré map for single ion motion subject to beating electrostatic waves. $\nu = 23.2$ and $\varepsilon = 10$ taken from Ref. 6. This cross-section occurs at the least common period between the two exciting waves.

a combination of numerical work and analytical theory examined the Poincaré map for ion motion subject to Eq. 7 in phase space for the case of off-resonance $\nu \neq m$ where m is an integer.[6] We show a sample Poincaré map in Fig. 7 where the time interval between points is equal to the shortest common period of the exciting waves. In this map, we see that ion motion is characterized by three separate regions, and the initial value of the Hamiltonian of an ion dictates in which region it will begin. The first acceleration zone, denoted the forbidden acceleration region, contains closed orbits about an elliptic point H_E that occurs where $(\theta, \rho) = (\pi, [\nu - \sqrt{\varepsilon}]/2,)$ in this cross-section or more generally where $\theta = \pi + \tau$. Physically, ions in this region experience an oscillation in their normalized Larmor radii about the elliptic point. In the stochastic acceleration region, ions are subject to a resonant interaction with the waves that is qualitatively similar to the stochastic acceleration found in single electrostatic wave (SEW) heating and described in great detail by Karney.[7] Particles in this region do not have closed orbits but rather experience incremental kicks in energy from the wave. The boundary between stochastic and acceleration regions is defined by the value $\rho = \nu - \sqrt{\varepsilon}$. In the third and final region, ions are subject to coherent acceleration until they pass the neighborhood of the hyperbolic point H_H at $(\theta, \rho) = (\pi, \nu - \sqrt{\varepsilon})$ in this cross-section, where again, more generally, $\theta = \pi + \tau$.

Once the ions pass this point, they in turn experience stochastic acceleration. The separatrix that separates the forbidden and regular acceleration regions is defined by the orbit that intersects H_H.

This phase portrait gives us vital information about the effect of initial conditions on ion energization and in particular demonstrates a means by which the normalized Larmor radius ρ can be increased. In order to fully explore the possible application to Fig. 6(b), however, we need to understand how BEW acceleration influences Y_{GC} as well. To this end, it is necessary to examine how and where in the orbit energy is exchanged with the exciting waves. We pursue this purpose both analytically and numerically. For the latter method, we used a symplectic integrator to solve the equations of motion governed by Eq. 8.

A. Regular and Forbidden acceleration

We show in Figs. 8(a) and 8(b) examples of ion motion corresponding to the initial conditions labeled in Fig. 7. For an ion initially in the forbidden acceleration region (Case a), we see the guiding center remains constant, and the Larmor radius oscillates on a timescale slower than the cyclotron period $\Delta\tau = 1$ about the elliptic point value, $\rho = [\nu - \sqrt{\varepsilon}]/2$. This is reminiscent of the linearized solution for any perturbed harmonic oscillator system about an elliptic point,[17] and it is physically the consequence of the coupling of the slow ion dynamics with the beat frequency, $(\nu_2 - \nu_1)/2 = 1/2$, generated by the two waves. The slow and continuous exchange of energy with the ion throughout the orbit prevents a preferential movement of the guiding center in any direction. The net effect then is the observed gradual increase in Larmor radius with fixed guiding center.

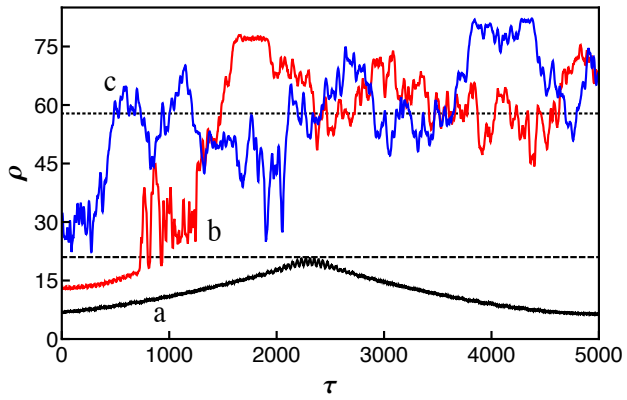

(a) Normalized radius ρ as a function of time. The dotted line corresponds to the average value achieved by ions that enter the stochastic region, ρ_h

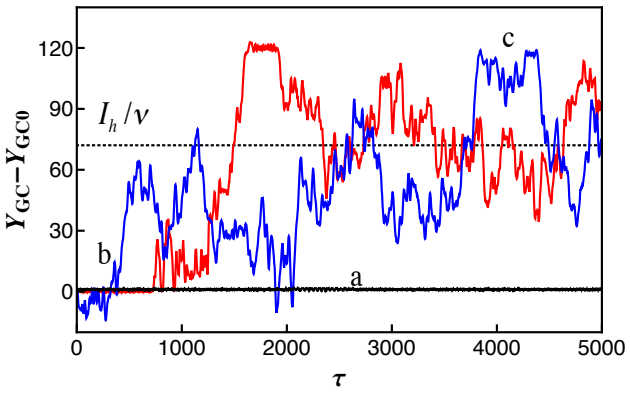

(b) Change in normalized y-coordinate of the guiding center as a function of time. The dotted line represents the average value, I_h/ν, achieved by ions in the stochastic region.

Figure 8. Sample trajectories for points shown in the Poincaré map in Fig. 7: a) Forbidden acceleration region; b) Regular acceleration; c) Stochastic acceleration. $\nu = 23.2$ **and** $\varepsilon = 10$**.**

For ions in the regular acceleration region (Case b), we observe that for an initial period, there is qualitatively similar behavior as in the forbidden region, i.e. a regular and coherent change in Larmor radius with fixed guiding center. However, the trajectory's oscillation about the elliptic point ultimately leads to $\rho = \nu - \sqrt{\varepsilon}$ at the hyperbolic point such that the ion enters the stochastic acceleration region. At this point the guiding center is no longer conserved and the Larmor radius starts to change chaotically. We will address this chaotic motion in the next section. For all ions coherently or regularly accelerated, however, before they reach the stochastic region, we can draw the following conclusions.

1. The y-element of the guiding center, Y_{GC}, remains fixed throughout the energy exchange.
2. The normalized Larmor radius ρ will increase or decrease in a systematic way depending on the initial phase.

B. Stochastic Acceleration

The stochastic acceleration region is characterized by a chaotic interaction between the exciting waves and ion motion. The coupling with ion dynamics therefore no longer depends on the beat frequency but rather on the phase velocity of the wave–just as in single electrostatic wave acceleration (SEW).[4] Following the treatment of Karney,[18] we can model this stochastic interaction with the waves as periodic kicks that occur when the phase velocity of one of the exciting waves and ion velocity in the wave direction are equal, i.e. when

$$\dot{X} = -\rho \sin\theta = \nu \tag{29}$$

where we have assumed that ν is sufficiently large such that $\nu_1 \approx \nu_2$. Outside this resonant condition, however, we note that the orbit remains largely unperturbed and therefore follows simple Larmor precession. During these unperturbed periods, the ion position is given from Eq. 19

$$\mathbf{R} = -\frac{B}{|B|}\left(V_{Y0}\hat{x} - V_{X0}\hat{y}\right) + \mathbf{R}_{GC} \tag{30}$$

where $\mathbf{R}$ is the position vector, V_{X0} and V_{Y0} are the normalized components of velocity in the $\hat{x}$ and $\hat{y}$ directions respectively, and $\mathbf{R}_{GC}$ is the position of the normalized guiding center. Since the energy exchange with the wave happens instantaneously and the ion resumes Larmor precession immediately after the exchange, we can describe the ion motion post-interaction as

$$\mathbf{R} = -\frac{B}{|B|}\left(V'_Y\hat{x} - V'_X\hat{y}\right) + \mathbf{R}'_{GC}. \tag{31}$$

where the primes denote the post-interaction values. From Eq. 29, we see that the interaction will only introduce velocity in the $\hat{x}$ direction such that $V'_X = V_X + \Delta V$ and $V'_Y = V_Y$. Equating Eq. 30 to Eq. 31, we thus see that

$$\Delta\mathbf{R}_{GC} \quad = \quad -\frac{B}{|B|}\Delta V\hat{y} \tag{32}$$

From this result, we confirm our assertion from Eq. 17 that the X coordinate of the guiding center remains constant, but the kicks result in a change in the guiding center in the $-\frac{B}{|B|}\hat{y}$. Moreover, these changes scale linearly with the increments in velocity, and we can relate this change to our normalized radius ρ. Specifically, we see that $\rho^2 = V_{X0}^2 + V_{Y0}^2$ and $\rho' = \left(V_{X0} + \Delta V\right)^2 + V_{Y0}^2$. But we take into consideration from Eq. 29 the fact that the kicks occur where $V_{X0} = \nu$ such that we find $\Delta V = -\nu + \sqrt{\nu^2 + 2\Delta I}$ where $I = \rho^2/2$ is a measure of the normalized kinetic energy. If we assume that the incremental changes are sufficiently small such that $\Delta I \ll \nu$, we thus find

$$\Delta V = \frac{\Delta I}{\nu} \tag{33}$$

This is the same result derived by Karney with energy considerations[19] and when summed over a series of steps allows us to approximate the position of the normalized guiding center as

$$Y_{GC} \quad = \quad Y_{GC0} - \frac{B}{|B|}\sum \Delta Y_{GC} \tag{34}$$

$$= Y_{GC0} - \frac{B}{\nu |B|} (I - I_0) \tag{35}$$

$$= Y_{GC} - \frac{B}{\nu |B|} \left(I - \frac{\rho_0^2}{2} \right) \tag{36}$$

Since the evolution of ρ and by extension I is inherently stochastic, it is difficult to predict the temporal dependence of both the guiding center and normalized Larmor radius. However, we can approximate the behavior by taking the time average of the motion such that

$$\langle Y_{GC} \rangle = Y_{GC0} - \frac{B}{\nu |B|} \left(\langle I \rangle - \frac{\rho_0^2}{2} \right). \tag{37}$$

Spektor and Choueiri estimated that $\langle I \rangle$ is a monotonically increasing function of ν, which Jorns and Chouieiri denoted $I_h(\nu) = \langle I \rangle$ where $I_h > (\nu - \sqrt{\varepsilon})^2 / 2$.[11,20] For convenience, we denote a new variable ρ_ν such that $I_h = \rho_h^2/2$. We thus find

$$\langle |Y_{GC}| \rangle = |Y_{GC0}| - \frac{1}{2\nu} \left(\rho_h^2 - \rho_0^2 \right). \tag{38}$$

From this expression, we can draw two definitive conclusions about ion motion for particles that are accelerated to the stochastic region from the regular acceleration region as well as those that start in the stochastic acceleration regime with $(\nu - \sqrt{\varepsilon}) < \rho_0$:

1. The normalized Larmor radius ρ will approach an average value ρ_h that increases monotonically with normalized frequency, ν.

2. The y-element of the guiding center, Y_{GC}, will move toward the average value given by Eq. 38, which translates to a net motion toward the magnetic null provided $\rho_0 < \rho_h$.

Case C in Figs. 8(a) and 8(b) illustrates both of these trends.

VI. Application of BEW acceleration to a magnetic slope

With our understanding of the different regimes of ion acceleration subject due to BEW, we next explore the effects of BEW acceleration in the presence of a magnetic slope. For this investigation, we assume the waves propagate with fixed k and ω_i uniformly in the plasma despite the changing magnetic field.

As can be seen from Fig. 6(b) and Eq. 15 expressed in terms of ρ and Y_{GC}, ions will be subject to forward-drifting orbits if they satisfy the criterion,

$$Y_{GC} - \frac{B}{|B|} \rho < 0. \tag{39}$$

While this quantity remains fixed in the absence of waves, as we showed in the previous section, BEW acceleration can change it. Our goal for the investigation of the BEW effect then is two-fold. First, for ions that start with $Y_{GC} - \frac{B}{|B|}\rho < 0$, will BEW acceleration push the ions into satisfying Eq. 39? And second, will the accelerated ions *remain* on average in this section?

To address these questions, we have taken Eq. 39 to hold initially and identified two regimes of behavior in Figure 9(a) distinguished by $|Y_{GC0}| < \nu - \sqrt{\varepsilon}$ in Figure 9(a) and $|Y_{GC0}| > \nu - \sqrt{\varepsilon}$ in Figure 9(b) where we have plotted $|Y_{GC}| - \rho$ versus normalized time. For the former, all ions outside the forward-drifting region necessarily have $\rho_0 < \nu - \sqrt{\varepsilon}$ such that they are all subject initially to coherent acceleration through either the regular or forbidden regions. As a consequence, there are two possible outcomes. On one hand, the ion starts in the forbidden acceleration region such that its normalized Larmor radius oscillates in time with fixed guiding center. However, the amplitude of the oscillation is such that for the entire orbit, $|Y_{GC}| - \rho > 0$, and these ions never enter a forward-drifting orbit. This is illustrated by the blue trajectory shown in Figure 9(a). The other outcome is that the ion starts with initial conditions that place it either in the regular acceleration region or forbidden such that it can be accelerated up to $\rho = |Y_{GC}|$. However, since these particles have not reached the stochastic regime $\rho = \nu - \sqrt{\varepsilon}$ at this point, they are still undergoing coherent acceleration. As a consequence of this well-behaved motion, we have found the interesting result that these regularly

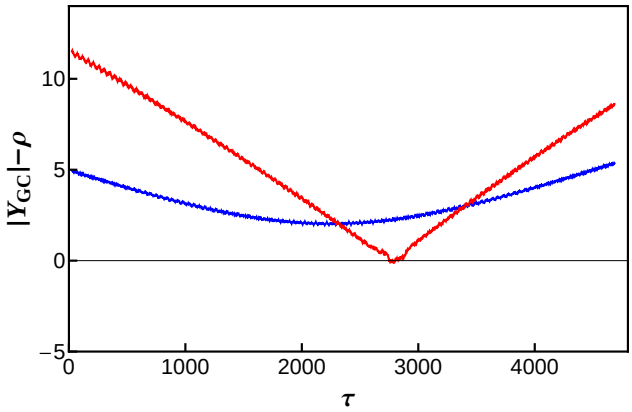

(a) $Y_{GC0} = 15$ such that $\nu - \sqrt{\varepsilon} > Y_{GC0}$ and all ions are trapped in closed Larmor orbits.

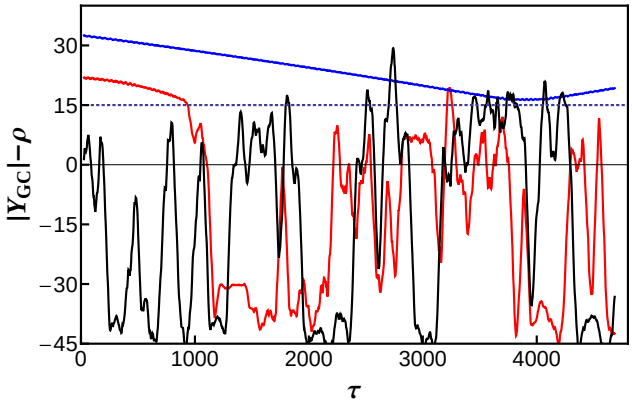

(b) $Y_{GC0} = 35$. Ions in the forbidden region cannot pass the dotted line where $Y_{GC} - \rho = \nu - \sqrt{\varepsilon}$. Ions starting below this line in the stochastic acceleration region and some starting above it in the regular acceleration regime are accelerated to and remain on-average in the forward drifting region.

Figure 9. $Y_{GC} - \rho$ as a function of normalized time τ. $\nu = 23.2$, and $\varepsilon = 10$. All initial conditions are chosen such that the ions start outside the forward-drifting region of Figure 6(b) where $|Y_{GC}| - \rho_0 > 0$. Ions enter forward-drifting regime when $Y_{GC} - \rho = 0$.

accelerated ions experience an immediate decrease in ρ at the magnetic null such that $|Y_{GC}| - \rho$ increases and they move away from the forward-drifting region. This is demonstrated by the red trajectory in Fig. 9(a). The qualitative explanation for this can be understood from the Poincaré map in Fig. 7 where we have already seen that in a homogenous magnetic field, ρ increases until the condition $\theta - \tau = \pi$ is satisfied and then begins to decrease after this point. In unnormalized parameters this condition is

$$\theta - \omega_c(y)t = \pi \tag{40}$$

where $\omega_c(y) = |qB(y)/m|$. We thus see at the magnetic null ($y = 0$) that $\omega_c(0) = 0$ such that Eq. 40 yields $\theta = \pi$. This, however, is precisely the angle the ion has from the $\mathbf{B} \times \mathbf{k}$ direction at the magnetic null. The particle consequently experiences an immediate deceleration in ρ such that it can never cross the $|Y_{GC0}| - \rho = 0$ bound. Coupled with our earlier observation, this result leads us to the conclusion that no ions initially in the Larmor region with $Y_{GC0} < \nu - \sqrt{\varepsilon}$ will be accelerated to forward-drifting orbits with BEW acceleration.

In Figure 9(b), we examine the case where $Y_{GC0} > \nu - \sqrt{\varepsilon}$ where the dotted line represents $\rho = \nu - \sqrt{\varepsilon}$. From this figure, we see three possible scenarios. In the first case, illustrated by the blue line, we see behavior similar to Fig. 9(a) in that ions are trapped in the forbidden acceleration region such that $\rho < \nu - \sqrt{\varepsilon}$, and therefore $|Y_{GC}| - \rho > 0$ for all time. These ions never pass into forward-drifting behavior. As a second case,

the black line, the ion starts in the stochastic region with $\nu - \sqrt{\varepsilon} < \rho_0 < \rho_h$ such that, as illustrated in the previous section, the ion has a net decrease in Y_{GC} and increase in ρ resulting in $|Y_{GC}| - \rho < 0$. The ions therefore do enter the forward-drifting region. As the third type of behavior, the blue line, we see that an ion that starts in the *regular* acceleration region with $\rho_0 < (\nu - \sqrt{\varepsilon})$ will be coherently accelerated to the stochastic regime where $Y_{GC0} = \rho$ and then in turn experience stochastic motion similar to that described above. Now, as illustrated above in Sec. V and Figure 7, the conditions on whether an ion will undergo forbidden or regular acceleration is dependent in a nonlinear manner on the initial conditions. However, in order to simplify our analysis, we make the same approximation as in Ref. 11 that ions with $\rho_0 > (\nu - \sqrt{\varepsilon})/2$, i.e. above the elliptic point H_E, are subject to regular and therefore stochastic acceleration. Therefore, we find that the necessary conditions for ions initially in the Larmor region to reach the forward-drifting zone are

$$\frac{1}{2}\left(\nu - \sqrt{\varepsilon}\right) < \rho_0 < |Y_{GC0}| \tag{41}$$

We further see that these orbits will *remain* on-average in this desirable region provided $|\langle Y_{GC}\rangle| - \rho_h < 0$ from Eq. 38. In terms of initial conditions, we can rewrite this as

$$|Y_{GC0}| < \rho_h + \frac{1}{2\nu}\left(\rho_h^2 - \rho_0^2\right) \tag{42}$$

which we in turn combine with Eq. 41 to yield the necessary conditions for ions to be accelerated to and stay in the forward-drifting region from the Larmor region:

$$\frac{1}{2}\left(\nu - \sqrt{\varepsilon}\right) < \rho_0 < |Y_{GC0}| < \rho_h + \frac{1}{2\nu}\left(\rho_h^2 - \rho_0^2\right). \tag{43}$$

where Eq. 39 is assumed to hold initially. Provided $\rho_h >> kL$, we can simplify this expression further by replacing the upperbound on $|Y_{GC0}|$ with the wall criterion such that we ultimately find

$$\frac{1}{2}\left(\nu - \sqrt{\varepsilon}\right) < \rho_0 < |Y_{GC0}| \tag{44}$$

where

$$\begin{cases} |Y_{GC0}| < kL - \rho_0 & \text{if } \rho_0 > \nu - \sqrt{\varepsilon}; \\ |Y_{GC0}| > kL - [\nu - \sqrt{\varepsilon}] & \text{if } \rho_0 < \nu - \sqrt{\varepsilon}; \end{cases}$$

The second condition on $|Y_{GC0}|$ for $\rho < \nu - \sqrt{\varepsilon}$ stems from the fact that initial regular acceleration does not produce a drift of the guiding center toward the magnetic null. As a consequence, the initial guiding center must be sufficiently far from the wall in order to guarantee the ion will still be in the geometry when ρ equals the threshold value. With this in mind, the above result represents the region of Larmor space that is enhanced to forward-drifting orbits by BEW acceleration.

Now, while it is apparent that BEW acceleration can augment the magnetic slope flow, there is still the possibility that the acceleration may push ions from the forward-drifting region into Larmor precession. We ask then, can ions with

$$|Y_{GC0}| < \rho_0 \tag{45}$$

be decelerated to the point that $\rho < |Y_{GC}|$? The answer we have found is invariably no. The reason for this is that initially forward-drifting orbits as showcased in Figs. 4(a), 4(b), 5(d), 5(e), and 5(f) advance considerably in $\hat{x}$ for each ion orbit. This has the net effect of randomizing the interaction with the BEW such that at each crossing of the magnetic slope, the ion has a new initial condition in the Poincaré map. This switching happens on the time scale of the cyclotron period $\Delta\tau = 1$ such that any coherent increase or decrease of the Larmor radius, which as we have already established happens on a much longer timescale, is not possible. Therefore, there is little net change in ρ and Y_{GC} such that these ions tend to remain in the forward-drifting section. The one exception to this is if the ion begins with initial conditions that result in $|\langle Y_{GC}\rangle| > \rho_h$ where Eq. 45 is also satisfied. In this case, as we see from Eq. 38, the particle will experience a net change in the guiding center away from the magnetic null and a decrease in the average Larmor radius such that it may become stuck on side of the magnetic slope. The criterion then for ions to remain in the forward drifting region–provided they start in it–is also given by

$$|Y_{GC0}| < \rho_h + \frac{1}{2\nu}\left(\rho_h^2 - \rho_0^2\right) \tag{46}$$

which again given that $\rho_h >> L$ and combined with the condition that the orbits initially be in the forward drifting region is

$$\begin{aligned} |Y_{GC0}| &< L - \rho_0 \\ |Y_{GC0}| &< \rho_0. \end{aligned} \tag{47}$$

This thus represents the other region of phase space that starts and will remain in forward-drifting orbits.

Enhanced drift from BEW acceleration

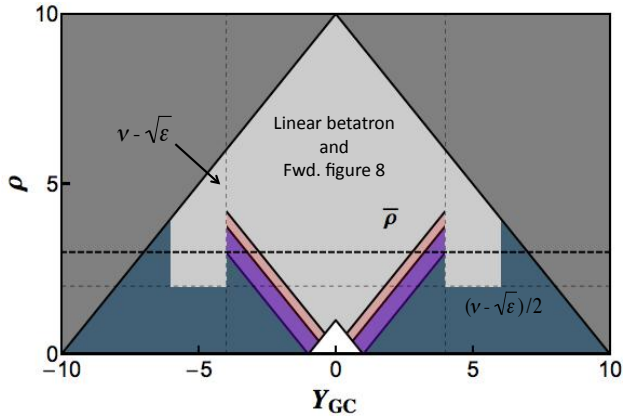

Figure 10. Portrait for enhanced drift in the magnetic slope due to BEW acceleration.

From the considerations of the previous sections, we use Eqs. 44 and 47 to compile an updated portrait of the regions of space susceptible to acceleration in Figure 10. Comparing to Fig. 6(b), we immediately see that for a fixed $\overline{\rho}$ more ions will undergo forward drifting acceleration than in the non-BEW case. We also emphasize here that provided $\overline{\rho} < \rho_h$, the net motion of the ions will be away from the walls toward the magnetic null–thus avoiding the losses associated with thermal heating. BEW acceleration clearly has the potential to be a mechanism for increasing the linear current along the magnetic null.

VII. Proof of concept design

With this mechanism for introducing a current in the $\hat{x}$ direction as well as a means for augmenting it with BEW current, we now turn our attention to a physical, concept that could exploit this ion flow for thrust. With this purpose in mind, we show in Fig. 11 a possible linear geometric configuration for a thruster proof of concept. This design has three major components: a plasma source (not shown), current sheets to provide a uniform magnetic field, and an inductive antenna for wave launching. We discuss each of these elements in detail.

1. Plasma source

Plasma generation is essential as a source of ions but in itself is only incidental to the acceleration process. Indeed, once the plasma is generated, it will diffuse from the source to the acceleration zone. Since the acceleration scheme relies on a stable magnetic gradient as well as BEW, the ideal plasma source for this concept is continuous with minimal interference with the waves in the acceleration zone. A low power helicon is one possible option.

2. Magnetic field configuration

The magnetic field configuration is essential for the acceleration process outlined above. In order to achieve the steep gradient as well as the null region, we arrange two parallel current sheets. The spacing between these must be sufficient in order to allow for wave excitation and propagation, i.e. $Lk \gg 1$

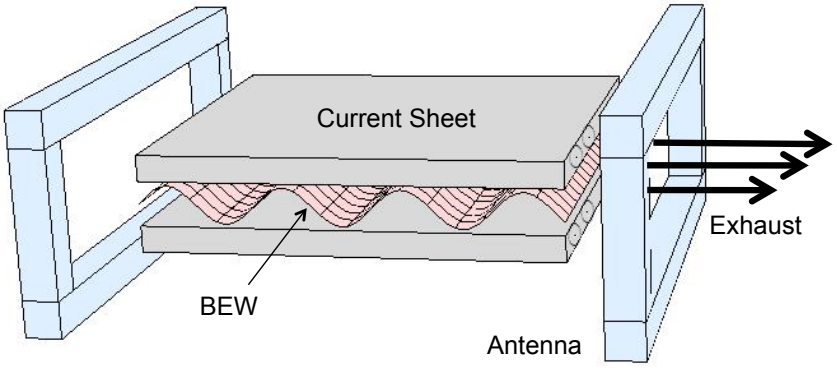

(a) Side view.

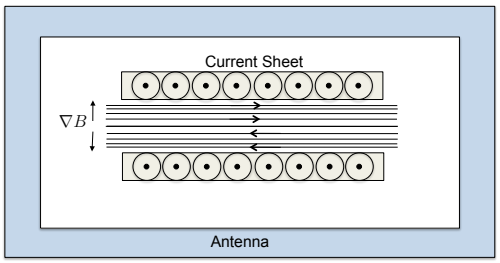

(b) Front view

Figure 11. Thruster concept with linear geometry. The current densities on the sheets are in the sme direction in order to produce a steep magnetic slope.

3. Inductive antenna

In order to generate the necessary BEW, we propose using the electrodeless, inductive antenna employed by Kline to launch electrostatic ion cyclotron waves.[21] The advantage of this element is that it consists of a two-coil, Helmholtz configuration (shown in Fig. 11), in which accelerated ions simply pass through one coil on exit of the thruster. This minimizes erosion of the thruster materials. Also, by properly aligning the coils to be colinear with the axis of the thruster, we can preferentially launch electrostatic waves in the necessary direction to achieve BEW augmentation of the ion drift.

Thruster operation

During operation of the thruster, plasma is generated at the source where it diffuses to the acceleration region that contains a magnetic slope similar in structure to the ideal type outlined in Eq. 3. The antenna excites BEW along the axis of the thruster and perpendicular to the magnetic field in the acceleration zone. The resulting interaction with the ions results in a net drift along the magnetic null region out of the thruster.

The phase velocity of electrostatic waves that couple with ion dynamics in most cases will be much smaller than the average electron velocity, $v_{T_e} \gg v_\phi$, such that the BEW will not have much of an effect on electron behavior. However, some electrons in the plasma by virtue of close proximity to the magnetic slope and appropriate initial velocity will be subject to the behavior outlined in Sec. II including linear betatron, figure-8, and grad-B trajectories with a reversed sign due to the change in charge. This will serve to further bias the exhaust of the thruster. The hope is that this charged plume will ultimately lead to an ambipolar field that will work to drag electrons with the propelled ions–thus preserving neutrality of the plume. However, particle-in-cell simulations may be necessary to fully elucidate this point.

VIII. Conclusion

In the above work, we have outlined the design for a new plasma thruster concept starting with the basic theory of operation and ending with a proposed proof of concept. Specifically, we demonstrated that in a rectilinear geometry, a sharp magnetic slope perpendicular to the direction of the magnetic full can result in a linear ion current. This is comparable to the current that forms along the magnetic null in an FRC plasma. We have further showed that BEW direct ion acceleration, as opposed to plasma heating, can considerably augment this acceleration while minimizing wall losses in order to produce a constant stream of ions in the magnetic null direction. In our final section, we proposed a proof of concept for a thruster design in order to investigate the efficacy of this acceleration mechanism for generating thrust. This BEW thruster thus shows promise as a new form of electric propulsion that bears further investigation through numerical simulations as well as experiment.

Appendix

We provide here a physical argument for the boundary in phase space between forward figure-8 and backward figure-8 orbits cited in Eq. 15. Specifically, we see that the linear betatron orbit transition occur where $P_X = 0$, which using our definition of Y_{GC} from Eq. 22 translates to

$$Y_{GC} = \frac{B}{|B|}\left(\overline{A}_X(k\delta) + k\delta\right). \tag{48}$$

This expression implies that the guiding center is on the *opposite* side of the magnetic null from where the particle is located (recall $B = B(y)$ and $\overline{A}_X(k\delta) + k\delta < 0$). On the other hand, the transition from grad-B to figure eight orbits occurs where $V_{eff}(0) = H$ which in physical space corresponds to

$$|Y_{GC}| = \rho + \left(\overline{A}_X(k\delta) + k\delta\right) \tag{49}$$

such that the guiding center is on the same side of the magnetic slope as where the particle is located. The transition from backward figure-8 to forward figure-8 must lie somewhere between the conditions described by Eqs. 48 and 50. We therefore place the transition from forward figure-8 to backward figure-8 at

$$|Y_{GC}| = \rho + \left(\overline{A}_X(k\delta) + k\delta(1-\alpha)\right) \tag{50}$$

where $0 < \alpha < 1$. Through modeling the trajectories numerically, we found $\alpha \approx 1/2$. This translates to the condition in energy space cited in Eq 15.

Acknowledgments

This project was initially supported by the Air Force Office of Scientific Research. It is currently carried out with assistance from the National Science Foundation and the Program in Plasma Science Technology, Princeton Plasma Physics Laboratory.

References

[1]Mozer, F., Carlson, C., Hudson, M., Torbert, R., Parady, B., and Yatteau, J., "Observations of paired electrostatic shocks in the polar magnetosphere," *Physical Review Letters*, Vol. 38, No. 6, 1977, pp. 292.

[2]Kintner, P., Kelley, M., Sharp, R., Ghielmetti, A., Temerin, M., Cattell, C., Mizera, P., and Fennell, J., "Simultaneous observations of energetic (kev) upstreaming and electrostatic hydrogen cyclotron waves," *Journal of Geophysical Research*, Vol. 84, No. A12, 1979, pp. 7201.

[3]Ram, A., Bers, A., and Benisti, D., "Ionospheric ion acceleration by multiple electrostatic waves," *J. Geophys. Res.*, Vol. 103, 1998, pp. 9431.

[4]Benisti, D., Ram, A. K., and Bers, A., "Ion dynamics in multiple electrostatic waves in a magnetized plasma. I. Coherent acceleration," *Physics of Plasmas*, Vol. 5, No. 9, 1998, pp. 3224–3232.

[5]Benisti, D., Ram, A. K., and Bers, A., "Ion dynamics in multiple electrostatic waves in a magnetized plasma. II. Enhancement of the acceleration," *Physics of Plasmas*, Vol. 5, No. 9, 1998, pp. 3233–3241.

[6]Spektor, R. and Choueiri, E. Y., "Ion acceleration by beating electrostatic waves: Domain of allowed acceleration," *Physical Review E*, Vol. 69, No. 4, April 2004, pp. 046402.

[7]Karney, C. and Bers, A., "Stochastic Ion Heating by a Perpendicularly Propagating Electrostatic Wave," *Physical Review Letters*, Vol. 39, No. 9, 1977, pp. 550.

[8]Spektor, R. and Choueiri, E., "Measurements of Ion Energization by a Pair of Beating Electrostatic Ion Cyclotron Waves," *International Electric Propulsion Conference Proceedings*, 2005.

[9]Spektor, B. and Choueiri, E., "Design of an Experiment to Optimize Plasma Energization by Beating Electrostatic Wave," *45th AIAA/ASME/SAE/ASEE Joint Propulsion Conference*, No. 5367, 2009.

[10]Spektor, B. and Choueiri, E., "Experiment for Plasma Energization with Beating Electrostatic Waves," *31st International Electric Propulsion Conference Proceedings*, No. 199, 2009.

[11]Jorns, B. and Choueiri, E. Y., "Ion Heating with Beating Electrostatic Waves," *Submitted for publication, June 15, 2010*, 2010.

[12]Fisch, N., "Theory of current drive in plasmas," *Review of modern physics*, Vol. 59, No. 1, 1987, pp. 175–234.

[13]Chia, P.-K., Schmitz, L., and Conn, R., "Stochastic ion behavior in subharmonic and superharmonic electrostatic waves," *Phys. Plasmas*, Vol. 3, No. 5, May 1996, pp. 1545.

[14]Landsman, A., Cohen, S., and Glasser, A., "Regular and stochastic orbits of ions in highly prolate field-reversed configutation," *Physics of Plasmas*, Vol. 11, No. 3, 2003.

[15]Hayakawa, Y., Takahashi, T., and Kondoh, Y., "Classification of particle orbits and stochasticity of plasma ion motion in a field-reversed configuration with D-^3He advanced fuel," *Nuclear Fusion*, Vol. 42, 2002, pp. 12–30.

[16]Strozzi, D. J., Ram, A. K., and Bers, A., "Coherent acceleration of magnetized ions by electrostatic waves with arbitrary wavenumbers," *Physics of Plasmas*, Vol. 10, No. 7, Jul 2003, pp. 2722–2731.

[17]Lichtenberg, A. and Lieberman, M., *Regular and Stochastic Motion*, Vol. 38 of *Applied Mathematical Sciences*, Springer-Verlag, New York, 1983.

[18]Karney, C., "Stochastic ion heating by a lower hybrid wave," *Physics of Fluids*, Vol. 21, No. 9, Sept. 1978, pp. 1584–1599.

[19]Karney, C., "Stochastic Ion Heating by a Lower Hybrid Wave: II," *Physics of Fluids*, Vol. 22, No. 11, Nov. 1979, pp. 2188–2209.

[20]Spektor, R., *Ion Acceleration by Beating Electrostatic Waves, Ph.D Thesis*, Vol. 1 of *Ph.D Thesis*, Princeton University, Princeton, NJ, 2006.

[21]Kline, J. L., Scime, E. E., Keiter, P. A., Balkey, M. M., and Boivin, R. F., "Ion heating in the HELIX helicon plasma source," *Physics of Plasmas*, Vol. 6, No. 12, Dec. 1999, pp. 4767–4772.